MISSOURI S&T

Missouri University of Science and Technology

Scholars' Mine

International Conferences on Recent Advances in Geotechnical Earthquake Engineering and Soil Dynamics

2010 - Fifth International Conference on Recent Advances in Geotechnical Earthquake Engineering and Soil Dynamics

28 May 2010, 8:30 am - 9:15 am

Performance-Based Design of Geotechnical Structures: Recent Advances

Susumu Iai
Kyoto University, Japan

Tetsuo Tobita
Kyoto University, Japan

Follow this and additional works at: https://scholarsmine.mst.edu/icrageesd

Part of the Geotechnical Engineering Commons

Recommended Citation

PERFORMANCE-BASED DESIGN OF GEOTECHNICAL STRUCTURES: RECENT ADVANCES

Susumu Iai
Disaster Prevention Research Institute
Kyoto University
Gokasho, Uji, Kyoto, 611-0011 Japan

Tetsuo Tobita
Disaster Prevention Research Institute
Kyoto University
Gokasho, Uji, Kyoto, 611-0011 Japan

ABSTRACT

The paper presents an overview of recent advances in earthquake geotechnical engineering with respect to the seismic design of geotechnical structures. The modern principles in seismic design are described along the framework of performance-based design as adopted in the International Standard (ISO23469). With the growing awareness of the need to understand the effect of non-linearity in soils and soil-structure interaction, the paper discusses the highly non-linear response of ground during strong earthquake motions with a peak ground acceleration exceeding 1g, and the highly non-linear behavior of soil-pile interaction, including soil-pile separation. The modern principles in seismic design described in this paper allow a sophisticated approach to deal with the uncertainty. Discussion on this issue is provided through the life-cycle cost approach. The paper also discusses the combined hazards, such as those during the Sumatra, Indonesia, earthquake of 2004, posing a new challenge to seismic design of geotechnical structures.

INTRODUCTION

The seismic performance of geotechnical structures is significantly affected by ground displacement. In particular, soil-structure interaction and effects of liquefaction play major roles and pose difficult problems for engineers. In spite of these facts, conventional seismic design of geotechnical structures was based on providing capacity to resist a design seismic force in a simplified manner. For example, the design seismic force was idealized through a specified seismic coefficient, typically ranging from 0.05 to 0.25 in coastal areas in Japan. The required capacity was determined to meet a specified margin of safety through a limit equilibrium analysis.

In the 1990's, the lessons learned from the earthquakes around the world having a peak ground accelerations ranging from 0.5 to 0.8g motivated an emergence of performance-based design (SEAOC, 1995; Iai and Ichii, 1998; Steedman, 1998). The goal was to overcome the limitations present in the conventional seismic design. If we demand that limit equilibrium not be exceeded in conventional design for the relatively high intensity ground motions associated with a very rare seismic event, the construction/retrofitting cost will most likely be too high. If force-balance design is based on a more frequent seismic event, then it is difficult to estimate the seismic performance of the structure when subjected to ground motions that are greater than those used in design.

In performance-based design, appropriate levels of design earthquake motions must be defined and corresponding acceptable levels of structural damage must be clearly identified (Iai, 2001). In 2002, a working group WG10 was established in TC98/SC3 in International Organization for Standardization (ISO) (see Acknowledgements for the list of working group members) for drafting a new International Standard that provides guidelines to be observed by experienced practicing engineers and code writers when specifying seismic actions in the design of geotechnical works. Seismic actions are generalized concept of seismic loads and include the actions due to ground displacement and soil liquefaction. Through the collective efforts of the working group members, a generalized methodology of performance-based design has been put together in the International Standard ISO23469 (ISO, 2005).

In order to present an overview of performance-based design and recent advances in geotechnical earthquake engineering, this paper first presents the modern principles in seismic design as adopted in this International Standard. The principles described in this International Standard are general enough to put various recent developments in geotechnical earthquake engineering in perspective. The paper reviews recent developments in evaluation of highly non-linear behavior of soils and geotechnical structures, including ground

response with a peak ground acceleration beyond 1g and soil-pile interaction with separation effects. The paper reviews the formal treatment of uncertainty in terms of a life-cycle cost approach. The new challenge to the geotechnical earthquake engineering is also discussed as posed by the combined hazards, such as those during the Sumatra, Indonesia, earthquake of 2004.

PRINCIPLES IN PERFORMANCE-BASED DESIGN

Following ISO23469, the principles in performance-based design may be summarized as follows (Iai, 2005).

In designing geotechnical structures, the purpose and functions are defined in accordance with broad categories of use such as commercial, public and emergency use. Depending on the expected functions during and after an earthquake, performance objectives for seismic design of geotechnical structures are generally specified on the following basis,
-   serviceability during and after an earthquake: minor impact to social and industrial activities, the geotechnical structures may experience acceptable residual displacement, with function unimpaired and operations maintained or economically recoverable after temporary disruption;
-   safety during and after an earthquake: human casualties and damage to property are minimized, critical service facilities, including those vital to civil protection, maintain full operational capacity, and the geotechnical structures do not collapse.
The performance objectives also reflect the possible consequences of failure.

For each performance objective, reference earthquake motion is specified as follows:
-   for serviceability during or after an earthquake: earthquake ground motions that have a reasonable probability of occurrence during the design working life;
-   for safety during or after an earthquake: earthquake ground motions associated with rare events that may involve very strong ground shaking at the site.

Based on the performance objectives and reference earthquake motions, performance criteria are specified in terms of engineering parameters that characterize the seismic response of and induced damage to geotechnical structures. The possible consequences of failure and type of analysis methods are considered in the formulation of the performance criteria.

In conventional seismic design, many factors that should be considered for design are specified rather than evaluated as described in the beginning of this paper. The principles in performance-based design described above are much more generalized and allow the experienced practicing engineers and code writers go back to the critical issues in design, including (1) purposes and functions of the facility, (2)

performance objectives for seismic design, reflecting the possible consequences of failure, (3) reference earthquake motions to be used for performance evaluation, and (4) performance criteria to specify the design parameters. For example, in the conventional seismic design of geotechnical structures, the consequences of failure are taken into account in terms of a factor specified in accordance with broad categories of importance. In the performance-based design, the consequences of failure may be evaluated, rather than specified, through a more sophisticated methodology. This aspect of performance-based design will be discussed later in this paper with respect to the performance objectives and uncertainty.

The performance objective apart, this International Standard classifies types of analyses of geotechnical structures for performance evaluation based on a combination of static/dynamic analyses and the procedure for soil-structure interaction as follows:
-   simplified: soil-structure interaction of a global system is modeled as an action on a substructure; the engineering parameters for specifying limit states are based on assumed failure modes and typically given in terms of margins to threshold limit, elastic limit, and approximate displacements and strains;
-   detailed: soil-structure interaction of a global system is modeled as a coupled system; the engineering parameters for specifying limit states are given in terms of both failure modes and extent of failure for non-linear dynamic analysis.

For example, in the simplified equivalent static analysis of a caisson quay wall, the model for analysis is defined for the wall as indicated by the shaded area in Fig. 1(a). Actions on this model are equivalent static inertia force, seismic earth and hydrodynamic pressures as indicated by the arrows in solid lines. The failure modes such as sliding, overturning, or bearing capacity failure are assumed in the analysis. The engineering parameters for specifying limit states for this model are the margin with respect to the threshold levels beyond which the wall begins to slide, overturn, or lose bearing capacity.

In detailed dynamic analysis of a caisson quay wall, a model for analysis is defined for an entire earth structure system, including the caisson, backfill soil, sea water, and foundation soil below the caisson as indicated by the shaded area in Fig. 1(b). Actions on this soil-structure model are input earthquake motions at the boundary of the domain of analysis as indicated by the arrow in solid line. The engineering parameters for specifying limit states for this model are responses of the soil-structure system, including accelerations, velocities, displacements, stresses and strains in various parts of the soil-structure system. In particular, seismic earth pressures and hydro-dynamic pressures acting on the caisson wall, as indicated by the arrows in dotted lines, are computed from, rather than specified for, the response analysis.
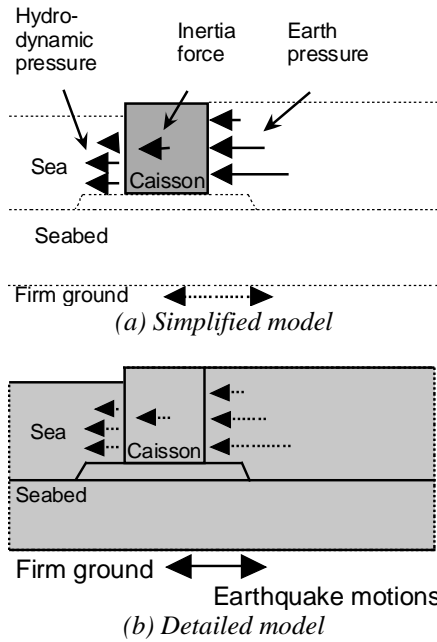
(a) Simplified model

(b) Detailed model

Fig. 1 Models of analysis for a caisson quay wall

These examples show how actions specified for designing a geotechnical structures and the engineering parameters for specifying limit states depend on the model of analysis. "A long history of confusion" as brilliantly put in "Fifty years of lateral earth support" (Peck, 1990) may be interpreted as the confusion caused by the problems associated with the (wrong) assumptions made on the failure mode or soil-structure interaction for the simplified model. It may be reasonable to repeat the well known, but often forgotten, fact that a simplified method is not a simple method; the method is born with a lot of insightful or bold assumptions made (sometimes "without explanation or apology," according to Peck (1990)) after enormous amount of studies and investigations to justify the assumptions. Facing with the highly non-linear response of soil-structure systems during strong earthquake motions recorded in recent years, we may well be going back to the basics of understanding the mechanism of soil-structure interaction as is rather than hastily jumping into adopting a simple method and trying to temper the model parameters in order to get the simple model fit the recorded case histories.

BACK TO THE BASICS: SOIL NON-LINEARITY

When a medium dense or firm ground is subject to moderate earthquake motions, soil behaves like linear material with reduced shear modulus and increased damping factor (Seed and Idriss, 1970; Zeghal et al., 1995; Yoshida and Iai, 1998). In these cases of mild non-linearity that is associated with the strain level in the order of magnitude less than about one percent, equivalent linear model has been often used in research and practice of seismic hazard analysis (Sugito et al., 1994; Dobry and Iai, 2000; NEHRP, 1997; Schnabel et al., 1972). However, when the ground is loose or soft or when the ground undergoes strong earthquake motions, soil non-

linearity becomes predominant and soil does not behave like linear or equivalent linear material. There is an increasing number of records of this distinctive non-linear behavior of soil. The strain level associated with this behavior is in the order of magnitude one percent or larger. As expected, the non-linear behavior of soil is closely related with failure mechanism of soil.

Isotropic linear elastic material

An isotropic linear elastic material, which plays a central role in seismology, is typically described as a linear relation between stress σ_{ij} (extension positive) and strain ε_{ij} (extension positive) as

$$\sigma_{ij} = C_{ijkl}\varepsilon_{kl} \tag{1}$$

$$C_{ijkl} = \lambda\delta_{ij}\delta_{kl} + \mu(\delta_{ik}\delta_{jl} + \delta_{il}\delta_{jk}) \tag{2}$$

where λ and μ are the Lame constants. Equation (2) is rewritten using bulk modulus K and shear modulus G as

$$C_{ijkl} = K\delta_{ij}\delta_{kl} + G(\delta_{ik}\delta_{jl} + \delta_{il}\delta_{jk} - \frac{2}{3}\delta_{ij}\delta_{kl}) \tag{3}$$

where

$$K = \lambda + \frac{2}{3}\mu \tag{4}$$

$$G = \mu \tag{5}$$

Substitution of Eq.(3) into Eq.(1) yields partition of the stress into those due to volumetric strain ε_{kk} and deviator strain $(\varepsilon_{ij} - \frac{1}{3}\delta_{ij}\varepsilon_{kk})$ as

$$\sigma_{ij} = K\delta_{ij}\varepsilon_{kk} + 2G(\varepsilon_{ij} - \frac{1}{3}\delta_{ij}\varepsilon_{kk}) \tag{6}$$

Thus, in an isotropic linear elastic material, volumetric strain produces hydrostatic (i.e. compression or extension) stress whereas deviator strain produces deviator stress. There is no coupling between the volumetric and shear mechanisms.

Non-linear material

Non-linearity in soil comes from two sources. One is the non-reversible stress strain behavior that is induced by the partial or total failure of the material. The other is the effect of pore water. Soil is an assembly of soil particles that forms a porous structure called soil skeleton. The pore of the soil skeleton is filled with water if the soil is below the ground water table. In the discipline of soil mechanics (Terzaghi, 1943), the total stress σ_{ij}, which is acting on an arbitrary plane within the soil, is partitioned into effective stress σ_{ij}' (extension positive), which is carried by the soil skeleton, and the pore water pressure $u\delta_{ij}$ (compression positive), as follows (see Fig. 2):
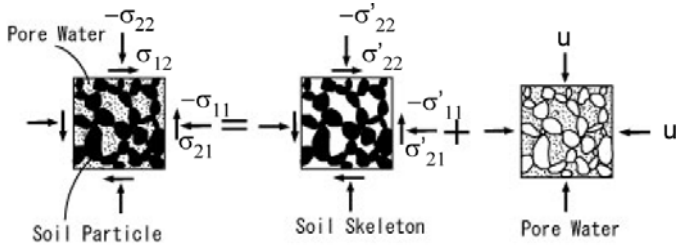
Fig. 2 Schematic figure for total stress, effective stress, and pore water pressure

$$\sigma_{ij} = \sigma_{ij}' - u\delta_{ij} \qquad (7)$$

Overall equilibrium equation of soil is satisfied for total stress σ_{ij} whereas deformation of soil is governed by the non-linear relation between the effective stress σ_{ij}' and strain ε_{ij} as

$$\mathrm{d}\sigma_{ij}' = D_{ijkl}'\mathrm{d}\varepsilon_{kl} \qquad (8)$$

Unlike the isotropic linear elastic material, soil exhibits coupling between the volumetric and shear mechanisms. This coupling mechanism is called dilatancy that may be attributed to the rearrangement of soil particles due to overall shear deformation as shown in Fig. 3 where the broken lines indicate original configuration of a soil element before shear. Thus, shear induces volumetric strain.

Fig. 3 Schematic figure for dilatancy (volume decrease due to shear)

Although dilatancy can be formulated through the tangential stiffness tensor D_{ijkl}' as is the case with elasto-plastic modeling, it is more convenient to explicitly write down the volumetric strain due to dilatancy $\varepsilon_0\delta_{kl}$ and rewrite Eq.(8) as follows:

$$\mathrm{d}\sigma_{ij}' = D_{ijkl}(\mathrm{d}\varepsilon_{kl} - \mathrm{d}\varepsilon_0\delta_{kl}) \qquad (9)$$

In this formulation, the coupling is reduced to the term $\varepsilon_0\delta_{kl}$, and therefore the stiffness tensor D_{ijkl} can be decoupled into those for volumetric and deviator mechanisms. In the strain space multiple mechanism model (Iai et al., 1992; Iai and Ozutsumi, 2005), this is written as

$$D_{ijkl} = K_{\mathrm{L/U}}\delta_{ij}\delta_{kl} + \frac{1}{4\pi}\iint G_{\mathrm{L/U}} \langle t_i, n_j \rangle \langle t_k, n_l \rangle \mathrm{d}\omega\mathrm{d}\Omega \qquad (10)$$

where t_i and n_i are contact normal (direction normal to the infinitesimal surface of a contact) and tangential direction (direction parallel to the infinitesimal surface of a contact) at each particle contact, and the tensor representing a virtual simple shear mechanism is given by

$$\langle t_i, n_j \rangle = t_i n_j + n_i t_j \qquad (11)$$

The integration is taken as a limit where the particle size are regarded as infinitesimally small for all the possible pair of t_i

and n_i. The angle ω is measured within each virtual plane spanned by a set of pairs of t_i and n_i sharing the same plane of two dimensional shear mechanism, and Ω is a solid angle associated with the normal direction to each virtual plane (see Fig. 4).
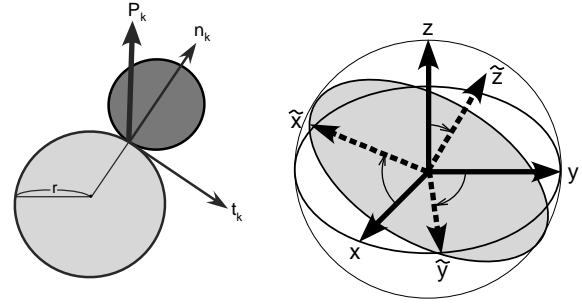

Fig. 4 Contact normal n_k, tangential direction t_k and contact force P_k defined at particle contact (left) and virtual plane of two dimensional shear mechanism defined by local coordinate indicated by the broken line vectors (right) (Iai and Ozutsumi, 2005)

In particular, the tangential bulk modulus $K_{\mathrm{L/U}}$ is defined by the current state and history of

$$\varepsilon = \delta_{kl}(\varepsilon_{kl} - \varepsilon_0\delta_{kl}) = \varepsilon_{kk} - 3\varepsilon_0 \qquad (12)$$

and each virtual shear modulus $G_{\mathrm{L/U}}$ is defined by the current state and history of

$$\gamma = \langle t_k, n_l \rangle(\varepsilon_{kl} - \varepsilon_0\delta_{kl}) = \langle t_k, n_l \rangle\varepsilon_{kl} \qquad (13)$$

The scalar γ is the projection of macroscopic strain field into the direction of virtual simple shear mechanism $\langle t_k, n_l \rangle$ and called 'virtual simple shear strain.' The subscripts L and U denote loading and unloading that are determined for isotropic mechanism by

$$\begin{aligned} \mathrm{d}\varepsilon &> 0 \quad \text{loading} \\ \mathrm{d}\varepsilon &= 0 \quad \text{neutral} \\ \mathrm{d}\varepsilon &< 0 \quad \text{unloading} \end{aligned} \qquad (14)$$

and for virtual simple shear mechanism by

$$\begin{aligned} \mathrm{d}\gamma &> 0 \quad \text{loading} \\ \mathrm{d}\gamma &= 0 \quad \text{neutral} \\ \mathrm{d}\gamma &< 0 \quad \text{unloading} \end{aligned} \qquad (15)$$

Integrated form of Eqs.(9) and (10) is obtained as

$$\sigma_{ij}' = p'\delta_{ij} + \frac{1}{4\pi}\iint q\langle t_i, n_j \rangle \mathrm{d}\omega\mathrm{d}\Omega \qquad (16)$$

where p' denotes effective mean stress, and q denotes virtual simple shear stress. They are defined by

$$\begin{aligned} \mathrm{d}p' &= K_{\mathrm{L/U}}\mathrm{d}\varepsilon \\ \mathrm{d}q &= G_{\mathrm{L/U}}\mathrm{d}\gamma \end{aligned} \qquad (17)$$

The history of dynamic effective stress analysis goes back to the same decade when the equivalent linear analysis was born in 1970's. The pioneering study of one dimensional effective

stress analysis was successful in idealizing the non-linear response of ground beyond one percent shear strain range, including generation and dissipation of excess pore water pressures in the ground (Finn et al., 1977). The strain space multiple mechanism model described here is one of the natural extension of this one dimensional model into general three dimensional stress space through the double integration in Eq. (10).

Although soil non-linearity is complex, its formulation has much in common with those with the isotropic linear elastic material. This fact may be understood by comparing Eqs.(1) and (3) with Eqs.(7), (9), and (10), or by comparing Eq.(6) with Eqs.(16) and (17). Difference can also be recognized; soil non-linearity is essentially anisotropic due to the structure of multitude of shear mechanisms, and effect of dilatancy predominates. These properties cannot be approximated by merely adjusting elastic moduli and damping factor in the isotropic linear elastic equation as is the case with the equivalent linear analysis.

An example of stress strain behavior of medium dense sand under cyclic loading is computed through the strain space multiple mechanism model, shown in Fig. 5. The shear strain in this figure is shown in decimal. As shown in this figure, general trend in the effective stress path is to gradually approach the state where the effective stress is zero (100% rise in excess pore water pressure). However, the medium dense sand exhibits dilative tendency and, as it strains beyond one percent range, it regains some stiffness and strength. If this strength is sufficiently large, it can transmit the large shear stresses and accelerations during strong earthquake motions.
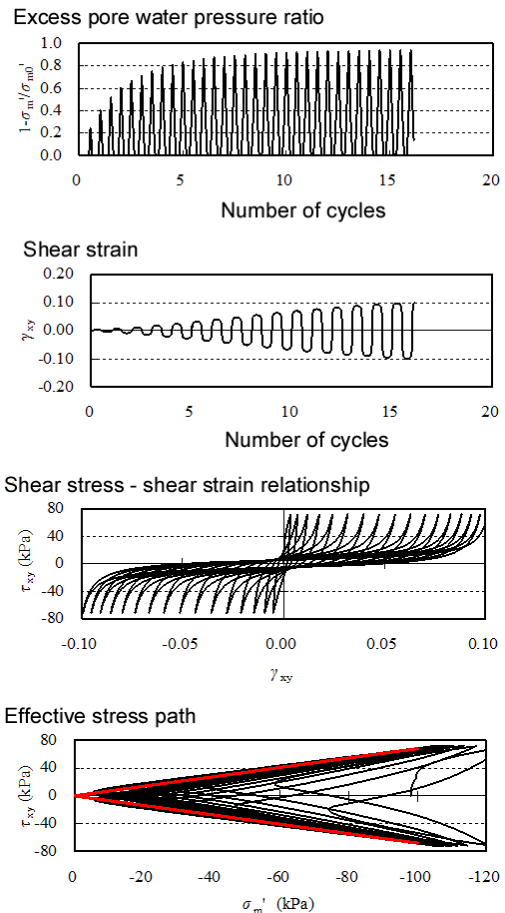
NON-LINEARITY IN SITE RESPONSE

The computed results shown in the previous chapter are the simplest case for demonstrating the effect of dilatancy on non-linear stress-strain behavior of soil that would be expected during strong earthquake motions. More and more data become available from the field to indicate the effects of dilatancy on the non-linear behavior of soil. An example, among others, is shown in Fig.6, where data are shown from borehole array in Kushiro Port, Japan, during the 1993 Kushiro-Oki earthquake (Iai et al., 1995). As shown in Fig.7, the strain space multiple mechanism model was successful in simulating the spiky acceleration response. The primary mechanism of this highly non-linear response is due to the stress-strain behavior of medium dense sand as shown in Fig.8.

Others reported in the literature (Porcella, 1980; Archuleta, 1998; Holzer et al., 1989; Zeghal and Elgamal, 1994) include data at Bonds Corner during the 1979 Imperial Valley earthquake, and data at the wildlife site during the 1987 Superstition Hills earthquake, shown in Figs. 9 and 10.

Fig. 5 Stress-strain behavior of medium dense sand

A more recent example, consisting of spike-like waves with a peak acceleration of 1.3g, from K-net site at Ojiya, Niigata, Japan, during the 2004 Niigata-ken Chuetsu earthquake, is shown in Fig. 11. An old example, but not yet received a wide recognition among the experts, is the data at Aomori Port, Japan, during the 1968 Tokachi-oki earthquake, shown in Fig. 12 (Tsuchida et al., 1969). Although the data from the Aomori Port was recorded through SMAC-B2 type accelerograph that tends to cut off high frequency component over 5 Hz, spiky waveform is still clearly recognized over duration of about 120 seconds.

This manifestation of non-linearity is different from the view based on the equivalent linear or non-linear models without the effect of dilatancy. In fact, the nonlinearity does not diminish the high frequency nature of the accelerograms, or necessarily reduce the peak acceleration (Archuleta, 1998). As manifested by the data from Ojiya site, the peak acceleration due to non-linear soil response can exceed 1g. The nonlinearity extends the duration of strong shaking as opposed to the commonly held view that nonlinearity will damp out the shaking and reduce the duration. The non-linear effect creates a record that has higher accelerations late in the shaking that are not included in the earthquake motion at the
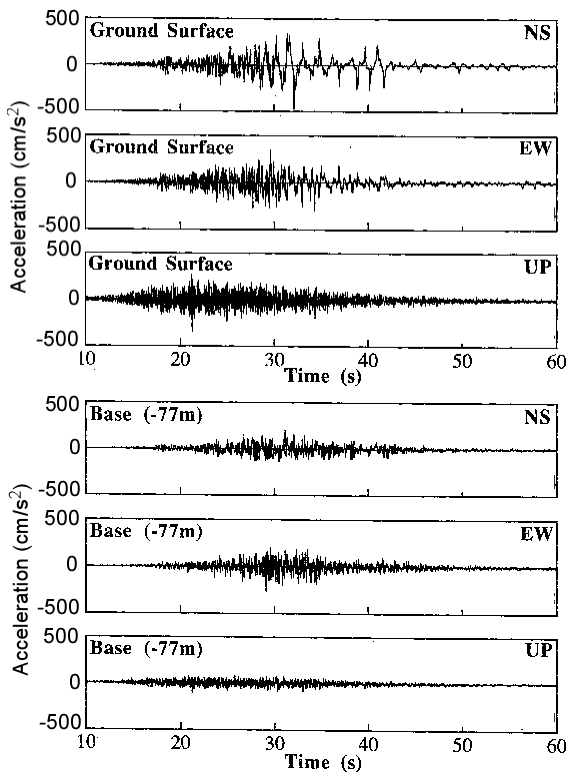
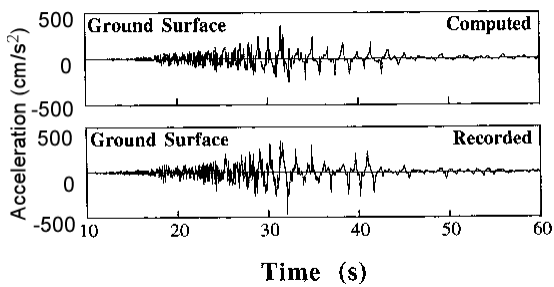*Fig. 6 Bore hole array data at Kushiro Port, Japan, during the 1993 Kushiro-Oki earthquake*

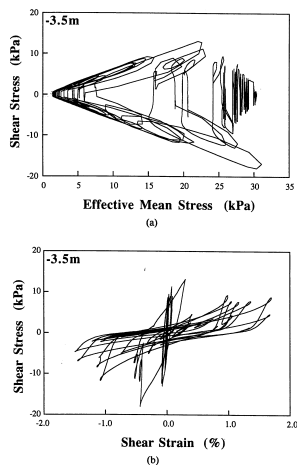*Fig. 7 Computed and recorded earthquake motions at ground surface at Kushiro Port, Japan*

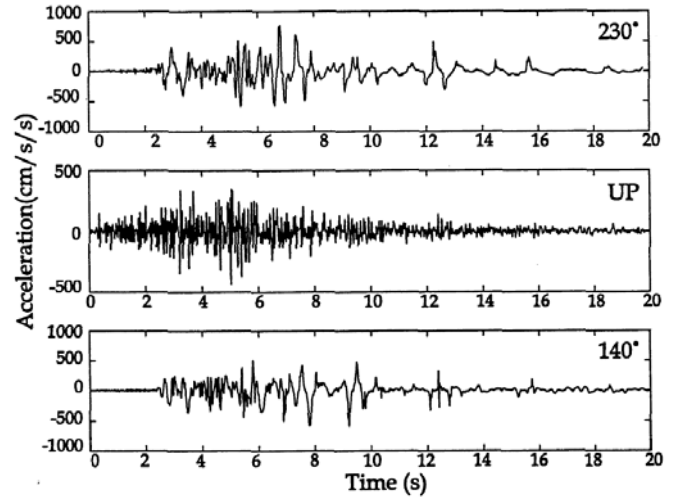*Fig. 8 Computed stress-strain behavior of soil*

Fig.9 Data at Bonds Corner during the 1979 Imperial Valley, USA, earthquake
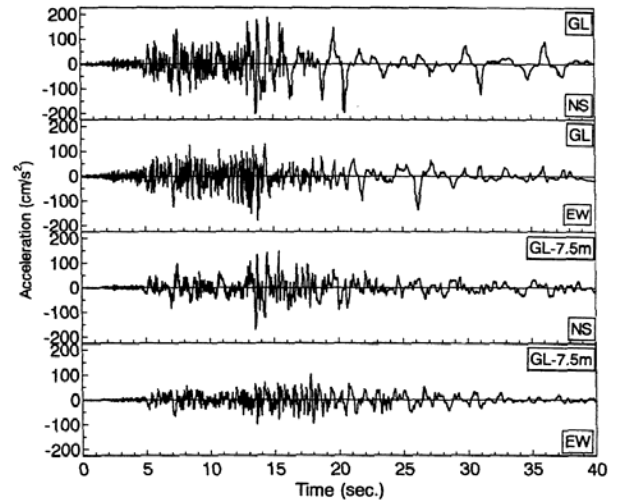

Fig. 10 Data at Wildlife site during the 1987 Superstition Hills, USA, earthquake
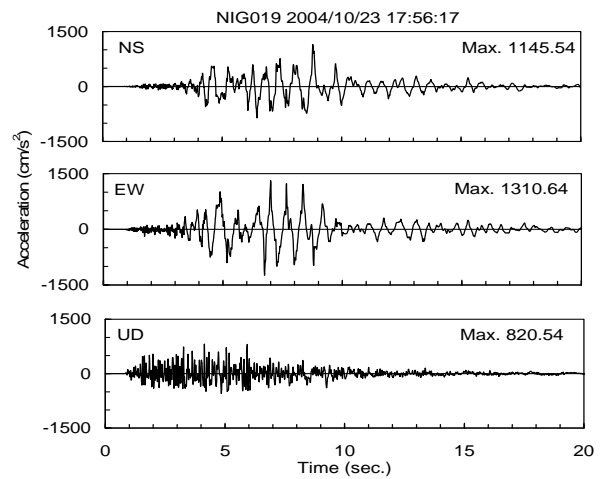

Fig. 11 Data at K-net Ojiya, Niigata, Japan, during the 2004 Niigata-ken Chuetsu earthquake (K-net, 2004)
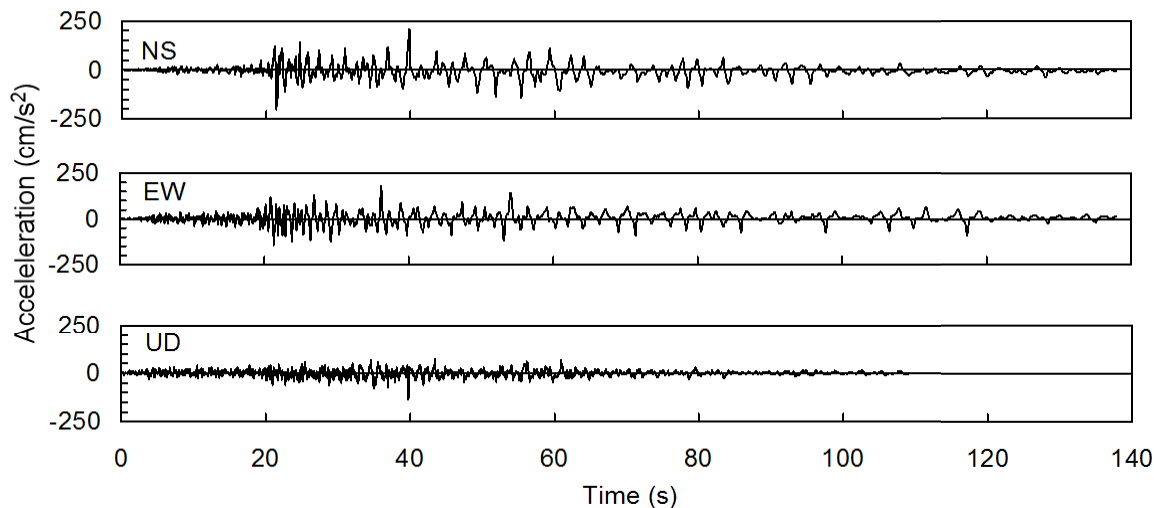
Fig. 12 Data at Aomori Port, Japan, during the 1968 Tokachi-oki earthquake

base but is associated with a long period motion that induces large strain in the soil deposit (Iai and Tobita, 2006).

The most recent addition to the non-linear response of soil is the non-symmetric vertical acceleration record at Ichinoseki-west, Japan, during the 2008 Iwate-Miyagi inland earthquake with a peak ground acceleration of 4g in vertical component (Aoi et al., 2008). The time history is shown in Fig. 13. Details on this record and the analysis are reported in a paper presented at this conference (Tobita et al., 2010).

The analysis using the input motions 0.7g in vertical component recorded at a depth of 260m uncovers that the mechanism of the strong non-symmetric vertical motion is due to the non-linear volumetric stress-strain relationship as shown in Fig. 14; dry soil cannot resist the tensile stress when the mass of subsurface soil is thrown upward whereas there is a sudden recovery of compressive stress when the soil mass comes back to push the earth along with the downward motion.
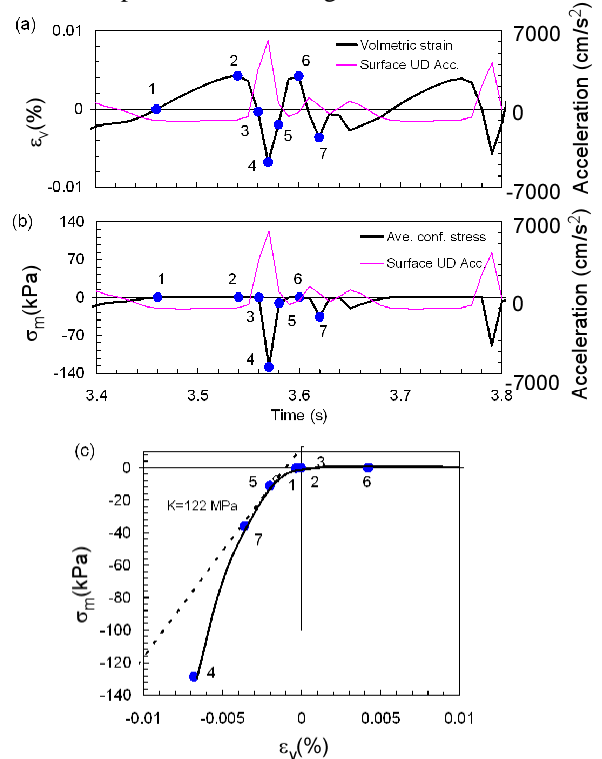
Fig. 14 Computed time histories from 4.5 to 5.0 (s); (a) volumetric strain, (b) mean stress. In (a) and (b), computed UD components of surface acceleration are plotted as a reference. (c) Mean stress versus volumetric strain relationship.

Fig. 13 Measured and computed acceleration at Ichinoseki-west, Japan, during the 2008 Iwate-Miyagi inland earthquake

NON-LINEARITY IN SOIL-PILE INTERACTION

Non-linearity in soil-structure systems subject to the strain levels beyond the mild non-linearity (i.e. beyond one percent strain range) poses difficult problems for engineers. In practice design, the non-linearity during earthquakes, including liquefaction, has been often dealt with a reduction factor applied to linear elastic parameters used for the static equilibrium analysis. In this practice, dynamic soil-structure interaction, including the kinematic interaction that may be induced by the large ground displacement, is often ignored. Although this practice may be beneficial to provide a certain extent of increase in capacity to resist the seismic actions, this practice is inappropriate in the understanding of the non-linear response and the failure mechanism of soil-structure systems subject to large strain levels. For performance-based design of geotechnical structures, where a certain degree of damage associated with the large strain is accepted, more studies are required to understand the non-linearity in soil-structure systems. In order to discuss this issue, a series of study on soil-pile interaction is reviewed below (Iai et al., 2009).

The series of the study began with the laboratory study on the local soil displacement field in the vicinity of the piles associated with a global displacement of soil around the pile foundation. A two dimensional model tests are performed on a horizontal cross section of a soil-pile system in a pile foundation (Iai et al., 2006). Silica sand No.7 was used in the model tests.

The local displacement field monitored through a video-camera was plotted in terms of displacement vectors at nodes of the grid formed by colored sand markers. Under saturated condition (Case-3), the displacement vectors were directed away from the front of the pile in a pattern of a fan as shown in Fig. 15 with a vortex type of displacement field at the pile side (upper side in the figure). The displacement vectors at pile side rapidly decreased with an increasing distance from soil-pile interface as shown in Fig. 16, both for dry and saturated conditions. The thickness of the transition zone where the shear strain is localized beside the pile is about 0.4mm. The shear strain level in this localized zone approaches 1000% level when the displacement of pile reached 4mm.
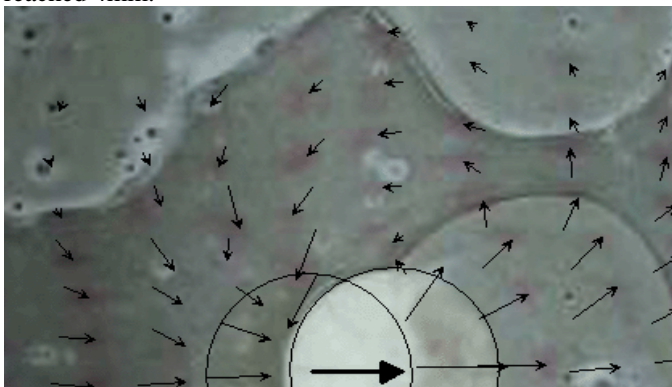

Fig. 15 Measured displacement field (pile displacement 21mm, load=6N) (Case-3: saturated)
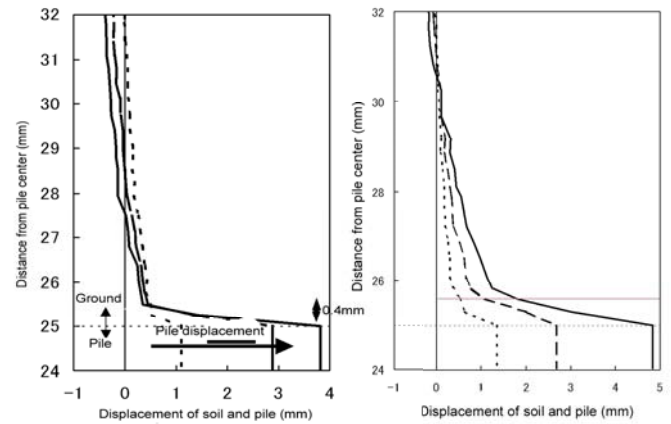

Fig. 16 Displacement distributions in the vicinity of soil-pile interface for dry and saturated sand deposits (Cases-1 and 3)

The strain localization in the vicinity of the pile side is due to the strong non-linearity of soil-pile interaction. The mechanism of this strong non-linear behavior will not be appropriately understood through the elastic analysis using a reduced modulus. The size of the finite element mesh in the vicinity of the pile, if the finite element analysis are used in the study, should be small enough to capture the strain localization.

Two dimensional analysis of a horizontal cross section of the soil-pile system was performed under pseudo-static conditions. An effective stress model based on the strain space multiple mechanism model was used. In this analysis, a single row of equally spaced piles deployed perpendicular to the direction of load (Fig. 17) was idealized into an analysis domain defined by the boundaries that run parallel to the load direction and go through the centers of the pile spacing. These boundaries were periodic, sharing the same displacements at the boundary nodes with the same x-coordinate, where x-axis is directed towards right on the paper. At the right and left side boundaries on the paper, x-displacements were fixed.

Finite element mesh used for the analysis of a single row of piles with a spacing of L=10D and a pile diameter D=5cm is shown in Fig. 18 for the area ranging from L=-5D to +5D. In the analysis, whole soil-pile system was initially consolidated with a confining pressure of 0.28 kPa for simulating the
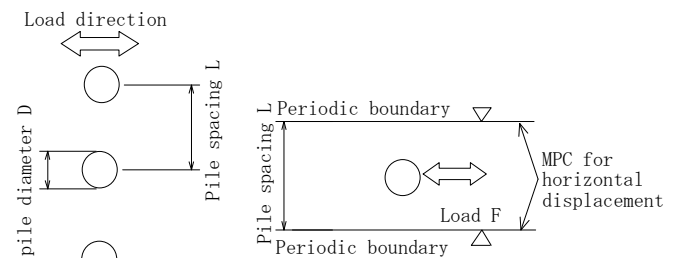
(a) Pile rows   (b) Analysis domain for single pile
Fig. 17 Two dimensional analysis of a soil-pile system in horizontal plane
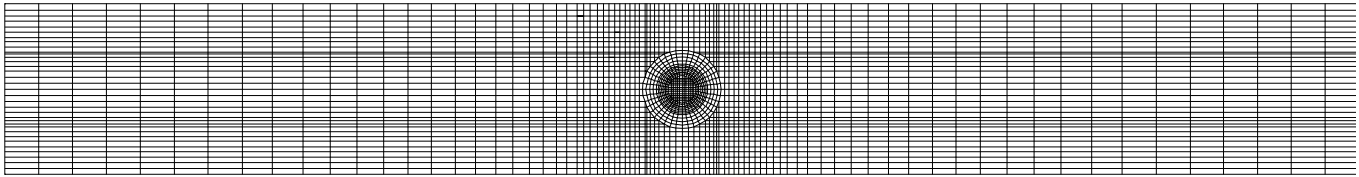
Fig. 18 Finite element mesh used for the analysis

confining condition at the middle depth of the model sand deposit (i.e. 2cm from the surface). Following this initial phase, a cyclic load was applied on the pile.

Computed displacement field for the saturated condition is shown in Fig. 19. Computed displacement distributions for dry and saturated conditions are shown in Fig. 20. The computed displacement field and the distributions are basically consistent with those measured in the laboratory and shown in Figs. 17 and 18. In particular, the analysis was successful in representing the shear strain localization at the pile side
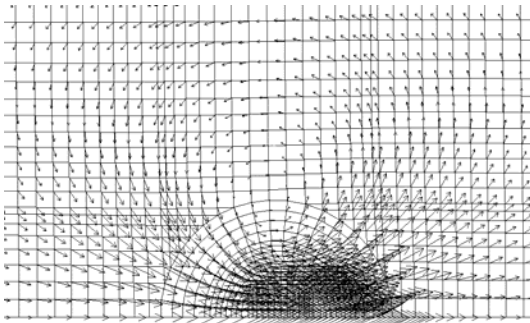
Fig. 19 Computed displacement field around pile (undrained) (Case-4)
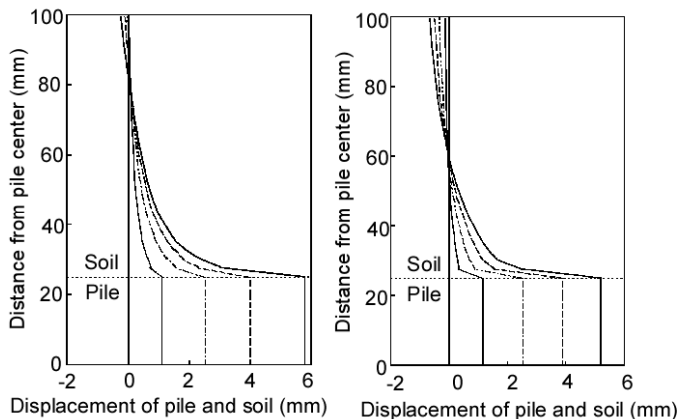
Fig. 20 Computed displacement distributions between the piles: (left) dry (Case-2), (right) saturated (Case-4)

By using the same mesh and parameters, the load-displacement relationship of a pile is computed for the horizontal cross section shown in Fig. 18 under dry and saturated conditions. The displacement is defined as that of the pile relative to that at the periodic side boundary that is located at the pile to pile center. In saturated condition, liquefaction front parameter S_0 was set equal to 0.05, which is equivalent to

the states of excess pore water pressure ratio of 0.95. The initial confining pressure used for the computation was 98 kPa for saturated sand. The finite element mesh used for the simulation was assigned for the diameter of pile equal to D=1m with a pile spacing of 2.5D, 5D and 10D.

Computed results for 5D for saturated condition are shown in Fig. 21. Although the computed load-displacement curves for dry condition (Iai et al., 2009) follows a typical shape of the p-y curve specified in the design recommendations, the load-displacement curve for saturated condition follows a hardening-spring type shape similar to the stress strain curve during cyclic mobility of saturated sands. These results show that the non-linearity in the load-displacement curves in a large strain range under saturated conditions should be more appropriately formulated than those adopted in the conventional design recommendations for designing pile foundations.

As a comparison, simple shear tests of a single element of soil were simulated using the same parameters as shown in Fig. 22.
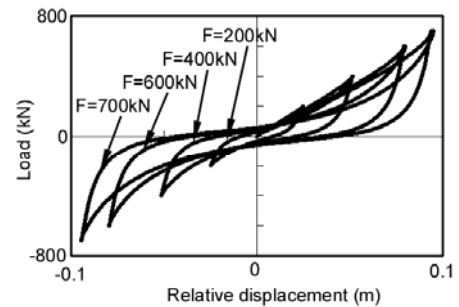

Fig. 21 Load-displacement relationship of pile-soil system in horizontal plane under cyclic loading
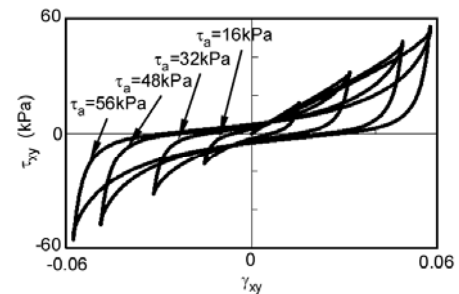

Fig. 22 Shear stress-shear strain relationship of a single soil element under cyclic simple shear

Although the mechanisms involved in the load-displacement curve are the results of complicated soil-pile interaction as exemplified by the local displacement field shown in Figs. 19 and 20, the load-displacement curves shown Although the mechanisms involved in the in Fig. 21 have practically the same shapes as those of the single soil element shown in Fig. 22.

There might be a several reasons for the similarity between the results of load-displacement relationship of pile-soil system and the shear stress-shear strain relationship of a single soil element. In this review paper, however, it may be sufficient to say that the similarity is confirmed for a wide range of pile spacing and geotechnical conditions. Based on the similarity between the results of load-displacement relationship of pile-soil system and the shear stress-shear strain relationship of a single soil element, the following relationships are derived (Ozutsumi, 2003) as follows:

$$\gamma_{xy} = u / (D\beta_p) \tag{18}$$

$$F = (LD\alpha_p)\tau_{xy} \tag{19}$$

$$\tau_{xy} = f(\gamma_{xy}) \tag{20}$$

where u denotes relative displacement, D denotes pile diameter, L denotes pile length, α_p=11.5 to 12.6, and β_p=0.5 (dry) to 2.5 (saturated) depending on the pile spacing and dry/saturated conditions. The path dependent function f in Eq.(20) is given by using a fictitious single soil element of the strain space multiple mechanism model.

For the analysis of pile-soil interaction during earthquakes, two dimensional analysis domain is set for a vertical cross section of soil-pile system. In this analysis, the soil-pile interaction in horizontal plane formulated through Eqs.(18) through (20) is idealized as a soil-pile interaction spring element as shown in Fig. 23. While the conventional spring elements used in the analysis of soil-pile interaction are embedded in the same plane of the two dimensional finite element analysis domain, the soil-pile interaction spring defined in this study is used as a spring that connects a free pile to a two dimensional cross section of soil between the piles. If looked in a plan view, the soil idealized through the finite element analysis is in a plane that goes along the periodic boundary line shown in Fig. 17(b) while the pile analyzed is located a part at a distance of a half pile spacing
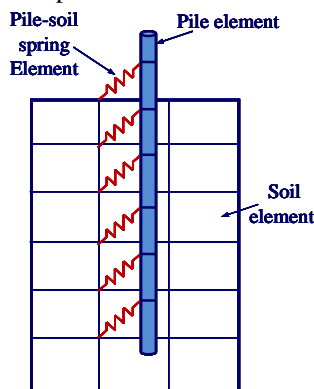

Fig. 23 Schematic figure of pile-soil interaction spring

EFFECTS OF SOIL-PILE SEPARATION

The strong non-linearity in soil-pile interaction arises not only from the non-linearity as discussed in the previous chapter but also from the soil-pile separation at large deflection level. This aspect of the non-linearity was studied through a two dimensional analysis of a full scale lateral loading tests of a 3 x 5 pile group performed at the Salt lake City Airport, USA (Rollins et al., 1998; Snyder, 2004). The soil profile consists of mostly clay having undrained shear strength ranging from 30 to 60 kPa. A sand layer mixed in the clay was located at a depth of 3 to 5 m having the internal friction angle of 38 degrees, whereas below 6m with 33 degrees.

For the full scale model tests, steel pipe piles were driven closed end to an embedment depth of 11.6m. The test pile has a 0.324 m outside diameter with a 9.5 mm wall thickness. The piles in the group were driven in a 3 x 5 patter with a nominal spacing of 3.92 pile diameters center to center in the loading direction and of 3.29 pile diameter perpendicular to it. The lateral load was applied 495 mm above the ground surface. A photograph of the overall layout of the 15-pile group, with a reference single pile in front, is shown in Fig. 24.

In the analysis of the full scale group pile test, finite element mesh shown in Fig. 25 was used for the computation. In this analysis, a joint element, having a properties shown in Fig. 26, is inserted between the corresponding nodes on the pile-soil spring and the pile element. The lateral load is statically applied at pile heads (0.495 m above the ground surface) until the displacement of 90 mm is achieved at the loading point.

Figure 27 shows computed and measured response of a single pile with and without soil-pile separation. The analysis without separation highly overestimates the lateral load-carrying capacity of the pile. In fact, the soil-pile gap was observed in-situ at the full scale test sites as shown in Figure 28. In the analysis, when soil-pile separation is considered, the load-deflection curve agrees well with those measured. The separation between soil and pile occurs in the analysis when the normal stress at the interface goes into tension regime. The

Fig. 24 Full-scale lateral load test layout; a reference single pile in front of 3 x 5 group pile(Snyder, 2004)
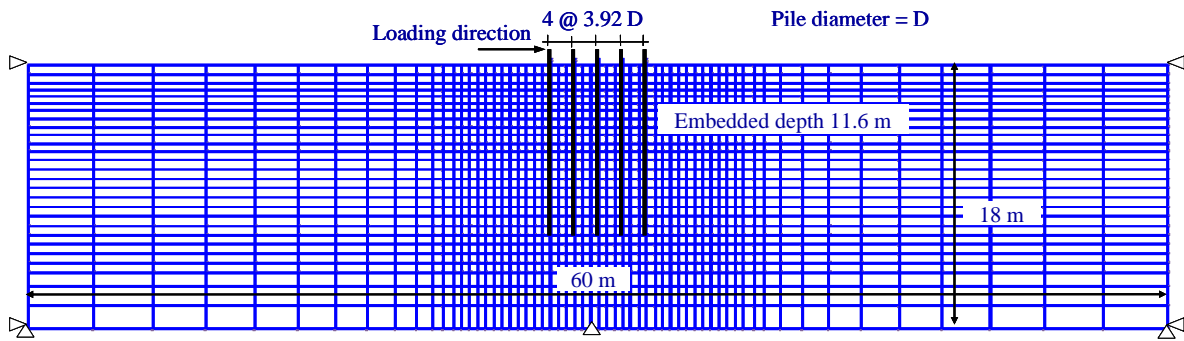
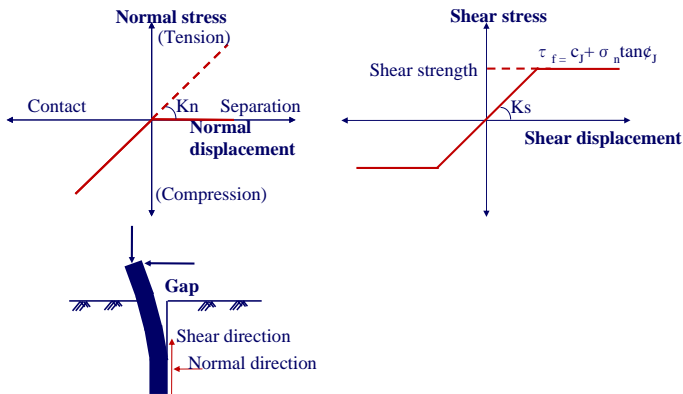*Fig. 25 Finite element mesh for the group pile under lateral load test*

Fig. 26 Schematic figure of join element for representing soil-pile interface effect
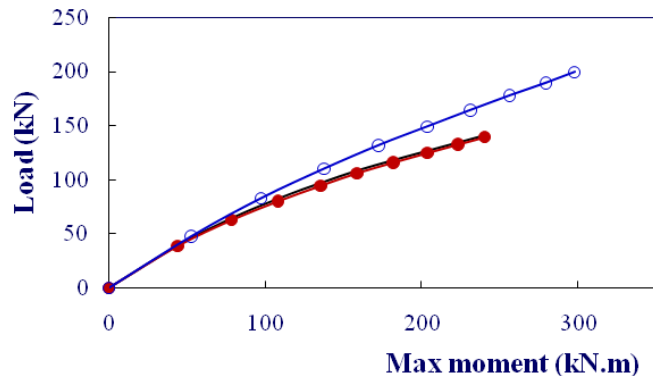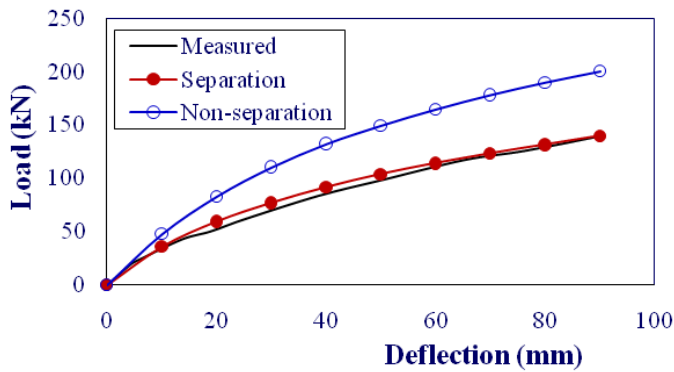

Fig. 27 Single pile response under static load: load-deflection curve (above), loading-maximum bending curve (below)
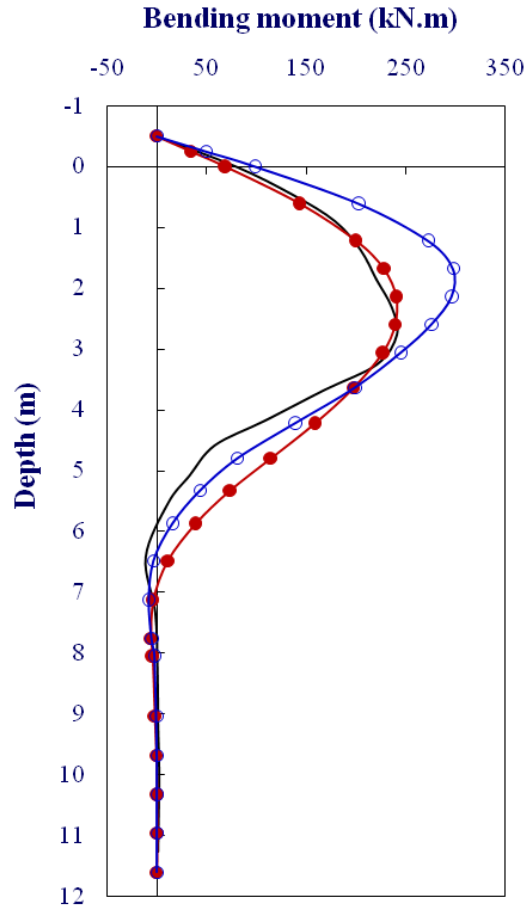

Fig. 27(continued) Bending moment distribution

computed load-maximum bending moment curve and the bending moment distribution with soil-pile separation also agree well with the measured. At the same load level, the analysis without soil-pile separation underestimates both deflection and maximum bending moment. At target deflection of 90 mm, ignoring soil-pile separation leads to 43% overestimation of the ultimate lateral load-carrying capacity of the pile.

Fig. 28 Photograph of a gap formation behind the pile (the pile is deflected laterally to the right and the gap is formed on the left of the pile in the photo) (Snyder, 2004)

Figure 29 shows the load distribution among the piles in pile group relative to the load of single pile at the same deflection levels. The distribution computed without the soil-pile separation effect shows minimum load at the middle pile, whereas that with soil-pile separation effect shows gradual decrease from the leading pile towards the trailing pile. The computed results with the soil-pile separation effect agrees well with those measured. The analysis without the soil-pile separation effect tends to exaggerate the load carried by the trailing pile (Iai et al., 2009).
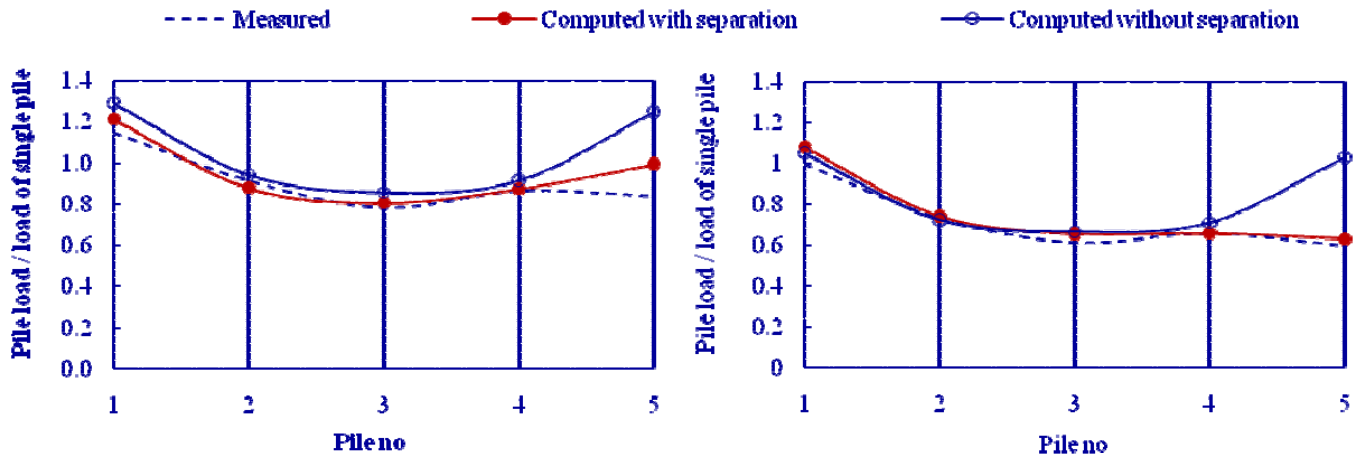
Fig. 29 Load distribution among piles in group pile; (left) at a pile deflection of 10 mm, (right) at 84 mm

PERFORMANCE OBJECTIVES AND UNCERTAINTY

As mentioned earlier, in conventional seismic design of geotechnical works based on the equivalent static method, the consequences of failure are taken into account in terms of a factor specified in accordance with broad categories of importance. In the performance-based design, the consequences of failure may be evaluated through a more sophisticated methodology. For example, acceptable levels of damage shown in Table 1 are specified by a combination of structural and operational damage. In this example, the consequences of failure are categorized into structural and operational aspects. Consequence of failure due to structural damage may be relatively easily evaluated based on the cost and time needed for repair of damaged structures. However, consequence of failure due to operational damage needs much more elaborate analysis, including systemic and financial analysis by viewing a geotechnical structure as a component of a larger infrastructure system.

Table 1 Acceptable level of damage in performance-based design*

Acceptable level of damage	Structural	Operational
Degree I : Serviceable	Minor or no damage	Little or no loss of serviceability
Degree II: Repairable	Controlled damage**	Short-term loss of serviceability***
Degree III: Near collapse	Extensive damage in near collapse	Long-term or complete loss of serviceability
Degree IV: Collapse****	Complete loss of structure	Complete loss of serviceability

* Considerations: Protection of human life and property, functions as an emergency base for transportation, and protection from spilling hazardous materials, if applicable, should be considered in defining the damage criteria in addition to those shown in this table.

** With limited inelastic response and/or residual deformation

*** Structure out of service for short to moderate time for repairs

**** Without significant effects on surroundings

While safety should be one of primary performance objectives for ordinary buildings, serviceability and economy become higher priority issues for ordinary geotechnical structures. For these structures, a methodology based on the principle of minimum life-cycle cost may be ideal (eg. Sawada, 2003). This methodology is emerging and will be eventually adopted as the state-of-practice in the coming decade.

Life-cycle cost is a summation of initial construction cost and expected loss due to earthquake induced damage. Probability

of occurrence of earthquake ground motion (i.e. earthquake ground motions with all (or varying) return periods) is considered for evaluating the expected loss due to earthquake induced damage. The life-cycle cost also includes intended maintenance cost and cost for demolishing or decommissioning when the working life of the structure ends.

When evaluating serviceability through life-cycle cost, failure of a structure is defined by the state that does not satisfy the prescribed limit states typically defined by an acceptable displacement, deformation, or stress. If a peak ground motion input to the bottom boundary of soil structure systems is used as a primary index of earthquake ground motions, probability of failure $F_F(a)$ at peak ground motion a is computed considering uncertainty in geotechnical and structural conditions. A curve described by a function $F_F(a)$ is called a fragility curve (Fig. 30(a)). Probability of occurrence of earthquake ground motions is typically defined by a slope (or differentiation) of a function $F_H(a)$ that gives annual probability of exceedance of a peak ground acceleration a. A curve described by a function $F_H(a)$ is called a seismic hazard curve (Fig. 30(b)).

Given the fragility and seismic hazard curves for a structure, annual probability of failure of the structure P_1 is computed as follows:

$$P_1 = \int_0^\infty \left(-\frac{dF_H(a)}{da} \right) F_F(a) \, da \qquad (21)$$

If a design working life is T years, probability of failure of the structure over the design working life is given by

$$P_T = 1 - \left(1 - P_1\right)^T \qquad (22)$$

If loss due to earthquake induced damage associated with the prescribed limit state is designated by c_D, expected loss over the design working life of a structure C_D is given by

$$C_D = P_T c_D \qquad (23)$$

Thus, the life-cycle cost C_{LC} is given by adding initial construction cost C_I, maintenance cost C_M and demolishing cost C_{END} as
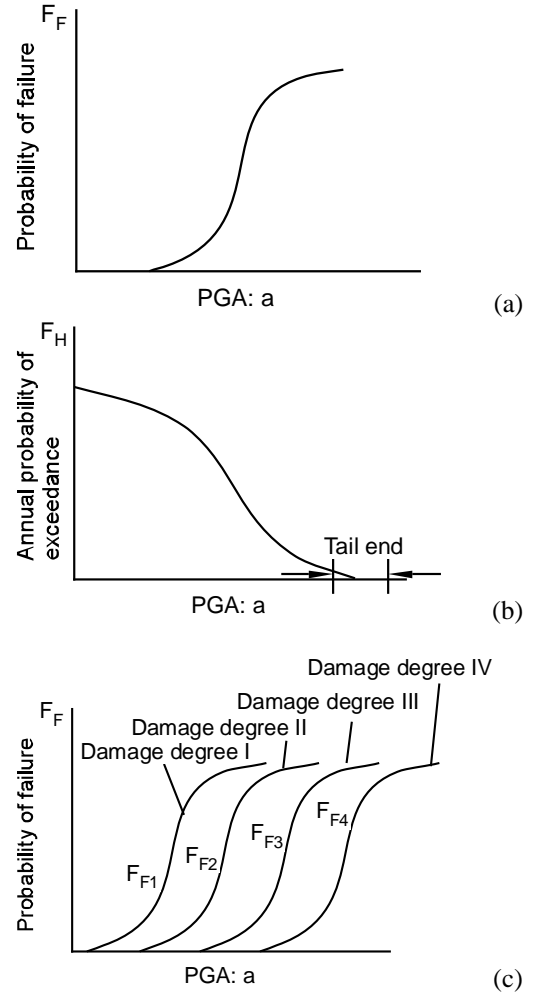
$$C_{LC} = C_I + C_D + C_M + C_{END} \qquad (24)$$

Fig. 30 Schematic figures of a fragility curve (a), a seismic hazard curve (b), and a group of fragility curves for multiple limit states (c)

This formulation is generalized further by introducing more than one serviceability limit state. Given the fragility curve defined for the ith limit state as $F_{Fi}(a)$ (Fig. 30(c)), Eqs.(21) through (24) are generalized as follows:

$$P_{1i} = \int_0^\infty \left(-\frac{dF_H(a)}{da} \right) F_{Fi}(a) \, da \qquad (25)$$

$$P_{Ti} = 1 - \left(1 - P_{1i}\right)^T \qquad (26)$$

$$C_{Di} = P_{Ti} c_{Di} \qquad (27)$$

$$C_{LC} = C_I + \sum_i C_{Di} + C_M + C_{END} \qquad (28)$$

As demonstrated for liquefaction hazard evaluation by (Kramer et al., 2006), the probability evaluated by Eqs.(21) and (22) is a consistent index of hazard and the conventional approach based on the return period prescribed in design provisions and codes can be either too conservative or unconservative depending on the site.

Expected loss evaluated by Eq.(23) is an index that reflects the consequence of failure. Life-cycle cost evaluated by Eq.(24) is an index that properly reflects the trade-off between initial

cost and expected loss. The design option that gives the minimum life-cycle cost is the optimum in terms of overall economy as shown in Fig. 31.

Thus, the optimum design has a certain probability of failure given by Eq.(22). This probability is not prescribed by an authority (such as 10% over 50 years) but rather determined as a result of the minimum life-cycle cost procedure. The probability of failure can be large if a consequence of failure in meeting the performance criteria, as measured by seismic loss c_D, is minor as shown in Fig. 32. The probability can be small, however, if a consequence of failure, as measured by c_D, is significant. Thus, the minimum life-cycle cost procedure reflects the possible consequences of failure and, thereby, satisfies the principles in performance objectives in the ISO guidelines described in the previous section (Iai et al., 2008).
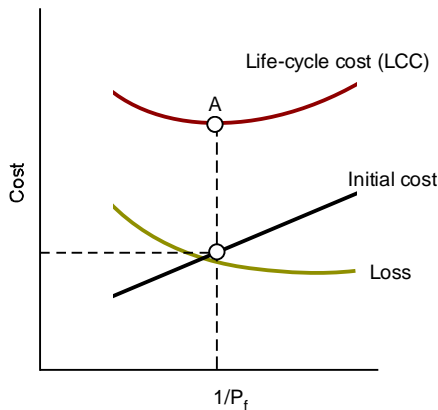
Fig. 31 Minimum life-cycle cost principle
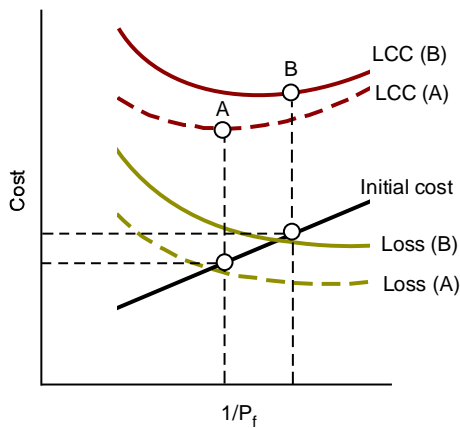
Fig. 32 Minimum life-cycle cost principle reflecting the consequence of failure

COMBINED HAZARDS

Rapid economic growth and urbanization in Asian countries have been noteworthy. Most of the developments are concentrated over coastal areas that are open to the sea for the advantages of development. These urban areas, however, are potentially vulnerable against earthquakes because they are developed over soft alluvial deposits. They are also vulnerable against flood due to high tide, typhoons, and tsunamis because of their proximity to the rivers and the sea. Rapid developments in these areas, far more rapid than those developments once achieved in Europe and North America, aggravate the situations against these natural hazards. A good urban planning and a solid engineering strategy are essential for preparing these areas against natural hazards. The Sumatra earthquake of 2004 reminded us the importance of our preparedness in coastal areas against natural hazards (Tobita et al., 2006).

The state-of-the-art earthquake engineering is typically based on site-by-site detailed analysis. A long coastal protection line poses a difficulty in directly applying the state-of-the-art earthquake engineering. A new methodology should be developed. A review is provided in this paper to discuss this issue based on the previous paper by the same authors (Iai and Tobita, 2007).

The coastal line, along which the seismic performance of geotechnical structures is evaluated, extends over 70km along Osaka Bay Area as shown in Fig. 33. As shown in this figure,
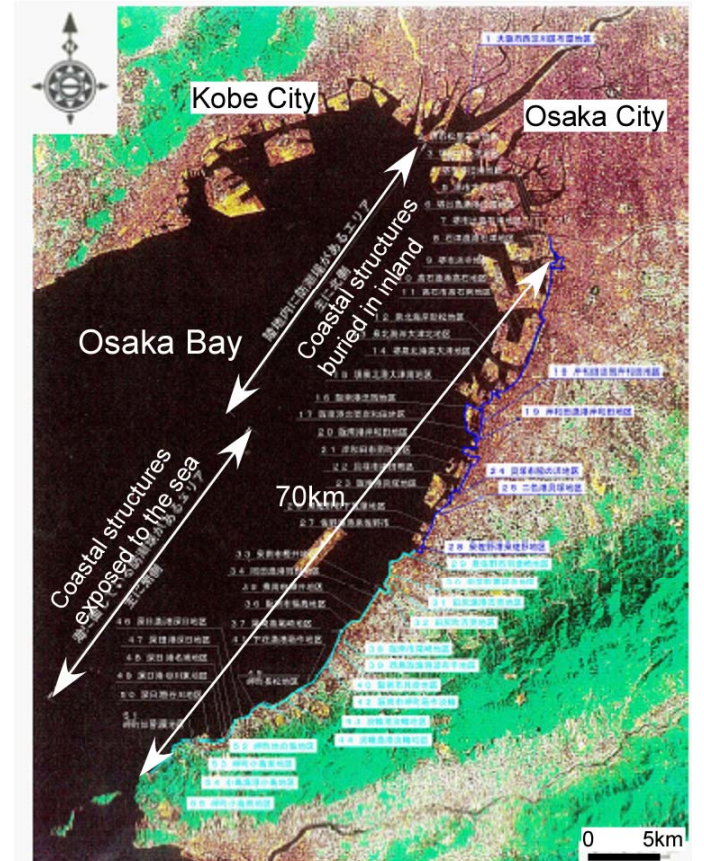

Fig. 33 Investigated coastal protection line for Osaka Bay Area, Japan
(Osaka_Municipal_Government, 2007)

northern part of the coastal protection line (designated by a blue line) is located slightly inland from the sea whereas southern part of the coastal protection line (designated by a green line) is exposed to the sea. Geotechnical conditions along the coastal protection line were compiled based on the boring data that were obtained at every 100 to 500m originally for the construction of the Hanshin Bay Area Highway.

Typical geotechnical profile consists of alternating layers of sand and clay deposit. Depth to the engineering base layer ranges from 10 to 80 m with a deepening trend toward north. Expected earthquake motions during the combined Tonankai and Nakai earthquakes of magnitude 8 class were set in four zones along the costal protection line with a peak accelerations ranging from 0.10 to 0.18g at the base layer for evaluation of seismic performance.

The primary objective of this assessment is to avoid the combined hazards such as those shown in Fig. 34.
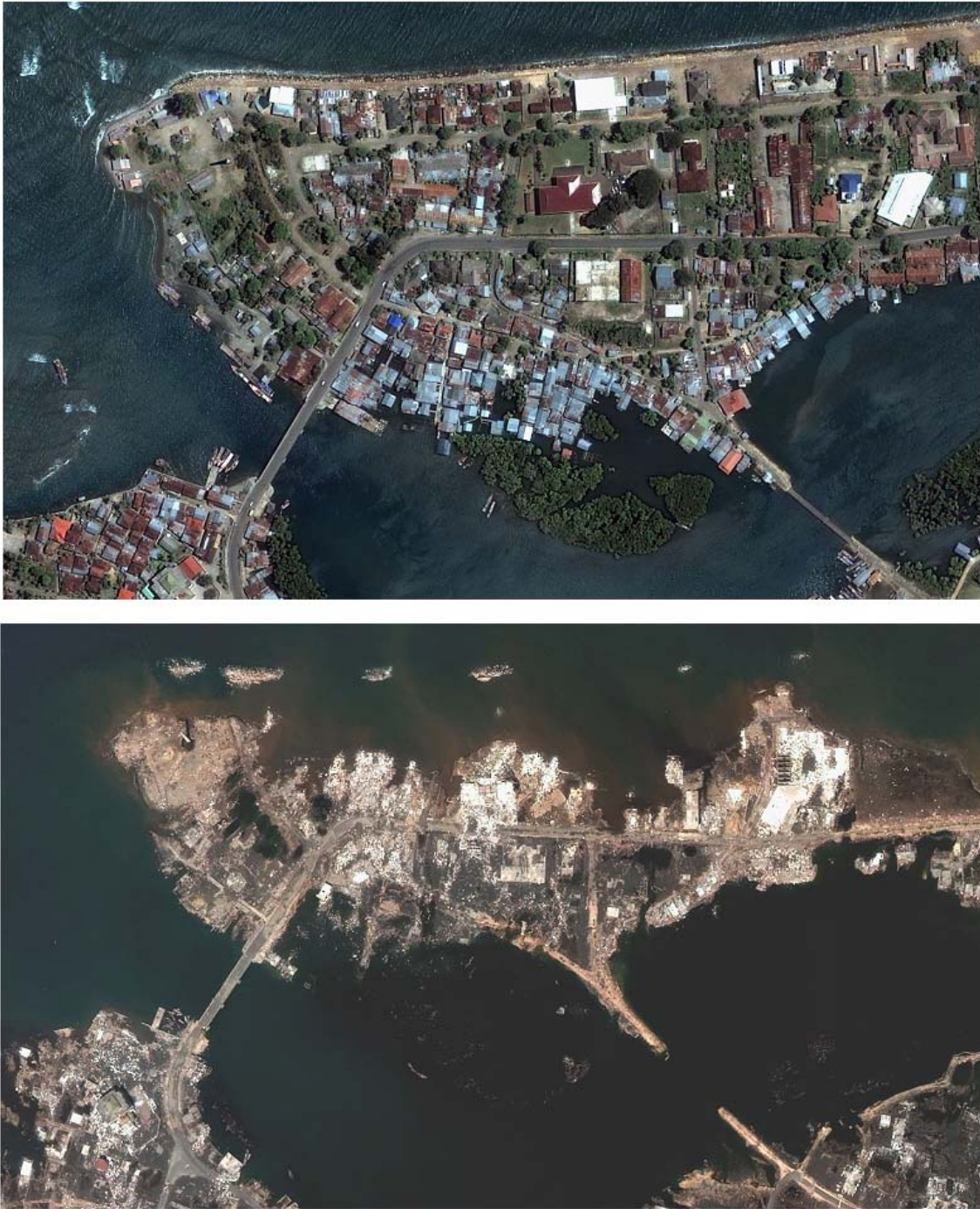
Figure 34 Coastal area of Banda Aceh, Indonesia, before (above) and after (below) the Indian Ocean-Sumatra earthquake of 2004 (after Quickbird)

The performance grades of the coastal structures that reflect the consequence of failure were specified based on two factors. One is the importance categorized by the level of the use of the land behind the coastal structures. If the level of the use of the land is high such as used for residence and/or industry, the consequence of the failure of the coastal structure becomes serious. If the level of the use of the land is low such as pastures and farmland, the consequence of the failure of the coastal structure may be not so serious.

The other is the elevation of the ground relative to the sea water level and expected height of the tsunami. If the elevation of the ground is lower than the sea water level (often called below zero meter area), the flood due to the failure of the coastal structure is very difficult to recover. If the elevation of the ground is higher the sea water level, the flood due to the failure of the coastal structure might be automatically recovered when the Tsunami or high tide are gone away.

The performance grades were specified based on a combination of these two factors and are designated as S, A, B, and C as shown in Fig. 35. These performance grades were used to specify the margin to allowable settlements of the coastal structures during the earthquake. For example, if the land behind the coastal structure is utilized for industry or residence and if the elevation of the land is lower than the sea level (HWL), such as shown in Fig. 36, and also illustrated in Fig. 35, performance grade is designated as S, the highest grade.

A set of design charts have been developed based on a series of parametric studies on embankments and gravity structures (Higashijima *et al.*, 2006). The cross sections and primary dimensions used as input parameters are shown in Fig. 36. Typical examples of the results of the parameter study are shown in Fig. 37. These results were compiled as a comprehensive set of data for the simplified design charts. These design charts are incorporated in a spread sheet format. Input data required are (1) basic parameters defining the cross section of structures, (2) geotechnical conditions as represented by SPT N-values, and (3) earthquake data, as represented by wave form, peak ground acceleration, or distance and magnitude from the seismic source. These design charts can be conveniently used for efficiently assessing the vulnerability of coastal geotechnical structures that extends a long distance, such as tens of kilometers, over a variable geotechnical and structural conditions.

Obviously each data point shown in Fig. 38 are the results of the seismic performance evaluation through the strain space multiple mechanism model; for a cross section of a dike shown in Fig. 39, the results are obtained as shown in Fig. 40(a), having a horizontal displacement of 30cm with a settlement of 3cm at the crest, or Fig. 40(b) of an idealized dike having the same cross section but with a foundation ground with SPT N-values of 10, having a horizontal displacement of 130cm with a settlement of 30cm at the crest. The failure mode of this dike can be characterized by a

relatively small settlement presumably because of the small size and light weight of the dike. If other cross section with heavier structure is analyzed, the settlement will be the dominant deformation mode. The simplified charts discussed above reflect these analysis results.
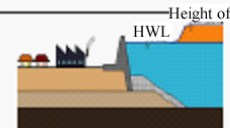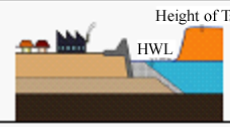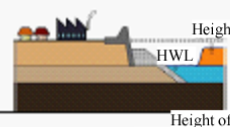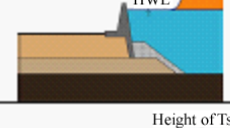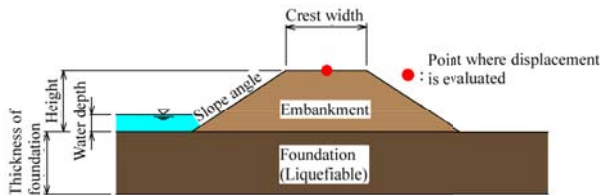

Fig. 35 Performance grades assigned for coastal structures ((Osaka_Municipal_Government, 2007)
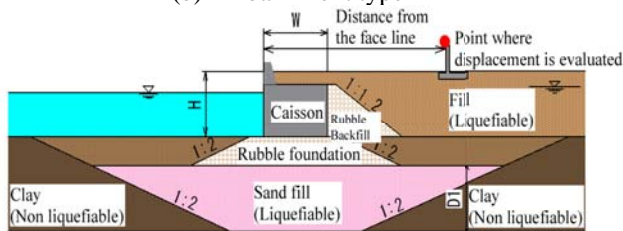

Fig. 36 Seismic damage to high tide protection wall in highly industrialized area during 1995 Kobe earthquake
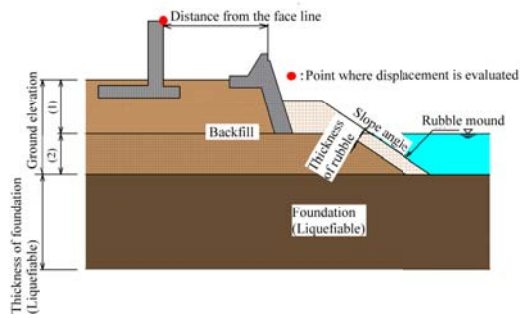
(a) Leaning bulkhead

(b) Embankment type

(c) Gravity type

Fig. 37 Cross sections and primary parameters used for the simplified design charts (Higashijima et al., 2006)
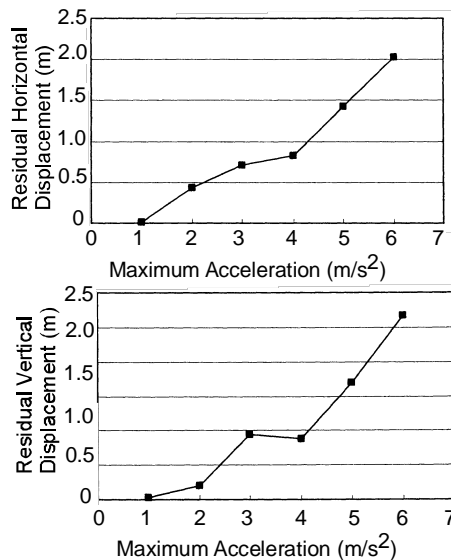

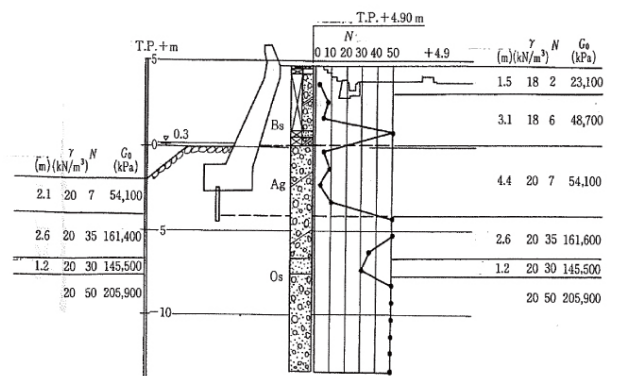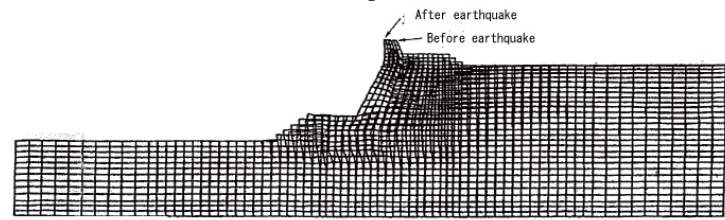*Fig. 38 Parameter study of displacements of leaning bulkheads over varying maximum accelerations*

Fig. 39 Example of cross section of a coastal geotechnical structure for assessment of seismic performance

Fig. 40 Computed residual deformation of a coastal geotechnical structure through effective stress analysis

The results of the seismic assessment of the coastal protection line in Osaka Bay Area are shown in Fig. 41. The settlements of the coastal protection facilities due to earthquake shaking ranged from 0.2 to 1.2m as shown in Fig. 41(a). Those settlements cause margin against Tsunami to be smaller. The areas that will not be able to protect the land from Tsunami and need strengthening or improvement for preparing against the Tsunami were identified from the results shown in Fig. 41(c).

Designing a large urban area against combined natural hazards poses a new challenge in earthquake engineering. The paper proposed the performance-based approach utilizing simplified design charts that are based on a parameter study of effective stress analyses of soil-structure systems. An application to the coastal protection line over a distance of 70km along Osaka Bay Area, Japan, demonstrates the efficiency of the proposed approach.
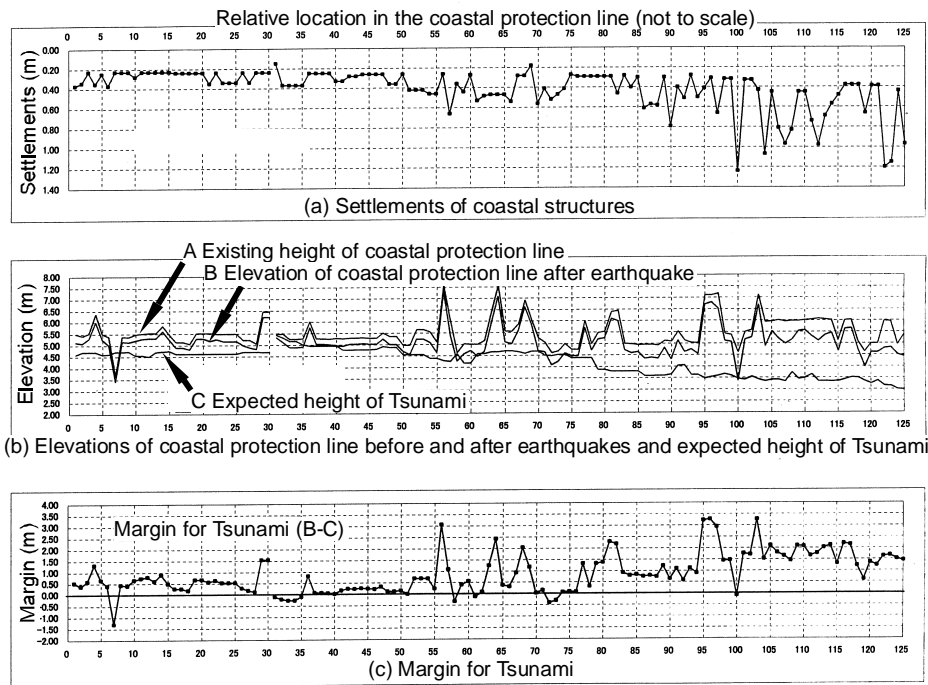
Fig. 41 Results of the seismic assessment of coastal protection line (Osaka_Municipal_Government, 2007)

CONCLUSIONS

An overview is presented on the recent advances in earthquake geotechnical engineering with respect to the seismic design of geotechnical structures. The primary implications from this overview may be summarized as follows:

(1) In conventional seismic design, many factors that should be considered for design are specified rather than evaluated. The principles in performance-based design presented in this paper are much more generalized and allow the experienced practicing engineers and code writers go back to the critical issues in design, including (a) purposes and functions of the facility, (b) performance objectives for seismic design, reflecting the possible consequences of failure, (c) reference earthquake motions to be used for performance evaluation, and (d) performance criteria to specify the design parameters.

(2) A confusion in the analysis for seismic design often arises from the problems associated with the (wrong) assumptions made on the failure mode or soil-structure interaction for the simplified model. It may be reasonable to repeat the well known, but often forgotten, fact that a simplified method is not a simple method; the method is born with a lot of insightful or bold assumptions made after enormous amount of studies and investigations to justify the assumptions. Facing with the highly non-linear response of soil-structure systems during strong earthquake motions recorded in recent years, we may well be going back to the basics of understanding the mechanism of soil-structure interaction as is rather than hastily jumping into adopting a

simple method and trying to temper the model parameters in order to get the simple model fit the recorded case histories.

(3) Strong non-linearity in site-response recorded through instruments during earthquakes is different from the view based on the equivalent linear or non-linear models without the effect of dilatancy. The non-linearity does not diminish the high frequency nature of the accelerograms, or necessarily reduce the peak acceleration. As manifested by the data from Ojiya site, Japan, during the 2004 Niigata-ken Chuests earthquake, or Ichinoseki-west site during the 2008 Iwate-Miyagi inland earthquake, the peak acceleration due to non-linear soil response can exceed 1g.

(4) Strong non-linearity in soil-pile interaction is identified as the manifestation of strain localization in the vicinity of the pile side. The mechanism of this strong non-linear behavior will not be appropriately understood through the elastic analysis using a reduced modulus. Load-displacement curves of a pile for saturated sand deposit follow a hardening-spring type shape similar to the stress strain curve during cyclic mobility of saturated sands. This fact directs us to a critical view on the conventional design recommendations for designing pile foundations. Another strong non-linearity comes from soil-pile separation occurring at a large displacement regime. The soil-pile separation can have a significant effect on the behavior of single and group piles.

(5) The modern principles in seismic design presented in this paper allow a sophisticated approach to deal with the uncertainty. The life-cycle cost approach is an promising

approach. The optimum design in the life-cycle cost approach has a certain probability of failure. This probability is not prescribed by an authority (such as 10% over 50 years) but rather determined as a result of the minimum life-cycle cost procedure. The probability of failure can be large if a consequence of failure in meeting the performance criteria is minor. The probability can be small, however, if a consequence of failure is significant. Thus, the minimum life-cycle cost procedure reflects the possible consequences of failure, offers a reasonable means of dealing with the uncertainty and, thereby, satisfies the modern principles of performance-based design described in this paper.

(6) Combined hazards, such as those at the 2004 Sumatra earthquake, poses a new challenge to the geotechnical earthquake engineers. The use of design charts, that reflect a series of comprehensive parametric studies based on the effective stress analysis, may be one of the efficient approach to meet this challenge.

ACKNOWLEDGMENTS

REFERENCES

Aoi, S., Kunugi, T. & Fujiwara, H. [2008]. "Trampoline effect in extreme ground motion," *Science,* Vol. 322, pp.727-730.

Archuleta, R.J. [1998]. "Direct observation of nonlinearity in accelerograms," *Second International Symposium on the Effects of Surface Geology on Seismic Motion,* Yokohama, Balkema, pp.787-791.

Dobry, R. & Iai, S. [2000]. "Recent developmnets in the understanding of earthquake site response and associated seismic code implementation," *GeoEng2000, An International Conference on Geotechnical & Geological Engineering,* Melbourne, Australia, pp.186-29.

Finn, W.D.L., Lee, K.W. & Martin, G.R. [1977]. "An effective stress model for liquefaction," *Journal of the Geotechnical Engineering Division, ASCE,* Vol.103, No.GT6, pp.517-533.

Higashijima, M., Fujita, I., Ichii, K., Iai, S., Sugano, T. & Kitamura, M. [2006]. "Development of a simple seismic performance evaluation technic for coastal structures," *2006 Ocean Development Symposium*, Japan Society of Civil Engineering.

Holzer, T.L., Youd, T.L. & Hanks, T.C. [1989]. "Dynamics of liquefaction during the 1987 Superstition Hills, California, earthquake," *Science,* Vol.244, pp.56-59.

Iai, S., Matsunaga, Y. & Kameoka, T. [1992]. "Strain space plasticity model for cyclic mobility," *Soils and Foundations,* Vol.32, No.2, pp.1-15.

Iai, S., Morita, T., Kameoka, T., Matsunaga, Y. & Abiko, K. [1995]. "Response of a dense sand deposit during 1993 Kushiro-Oki earthquake," *Soils and Foundations,* Vol.35, No.1, pp.115-131.

Iai, S. & Ichii, K. [1998]. "Performance based design for port structures," *Proc. UJNR 30th Joint Meeting of US-Japan Panel on Wind and Seismic Effects,* Gaithersburg, NIST, pp.1-13 (3-5).

Iai, S. [2001]. "Recent studies on seismic analysis and design of retaining structures," *Proc. 4th International Conference on Recent Advances in Geotechnical Earthquake Engineering and Soil Dynamics,* San Diego, pp.1-28 (SOAP4).

Iai, S. [2005]. "International standard (ISO) on seismic actions for designing geotechnical works - An overview," *Soil Dynamics and Earthquake Engineering,* Vol.25, pp.605-615.

Iai, S. & Ozutsumi, O. [2005]. "Yield and cyclic behaviour of a strain space multiple mechanism model for granular materials," *International Journal for Numerical and Analytical Methods in Geomechanics,* Vol.29, No.4, pp.417-442.

Iai, S. & Tobita, T. [2006]. "Soil non-linearity and effects on seismic site response," *Proc. 3rd International Symposium on the Effects of Surface Geology on Seismic Motion,* Grenoble, France, pp.21-46.

Iai, S., Tobita, T., Donahue, M., Nakamichi, M. & Kaneko, H. [2006]. "Soil-pile interaction in horizontal plane," *Geotechnical Special Publication 145, ASCE*, pp.38-49.

Iai, S. & Tobita, T. [2007]. "Seismic assessment of coastal structures against combined hazard with Tsunamis," *Proc. 8th Pacific Conference on Earthquake Engineering,* Singapore.

Iai, S., Tobita, T. & Tamari, Y. [2008]. "Seismic performance and design of port structures," *Geotechnical Earthquake Engineering and Soil Dynamics VI, Geotechnical Special Publication 181, ASCE*, pp.1-16.

Iai, S., Tobita, T., Hussien, M.N., Rollins, K.M. & Ozutsumi, O. [2009]. "Soil-pile interaction under lateral load," *Proc. International Workshop on Soil-foundation-Structure Interaction 2009,* Auckland.

ISO [2005]. "Bases for design of structures - Seismic actions for designing geotechnical works," *ISO23469*, pp.1-77.

Kramer, S.L., Mayfield, R.T. & Anderson, D.G. [2006]. "Performance-based liquefaction hazard evaluation: implications for codes and standards," *8th U.S. National Conference on Earthquake Engineering,* San Francisco, Paper No.888.

NEHRP [1997] "*Recommended provisions for seismic regulations for new buildings and other structures,*" Building Seismic Safety Council (BSSC), FEMA 203/303, Part 1 (Provisions) and Part 2 (Commentary)

Osaka_Municipal_Government [2007] "*Report of the Technical Committee for Seismic Assessment of Coastal Structures in Osaka Bay Area,*" Osaka

Ozutsumi, O. [2003]. "Numerical studies on soil-structure systems on liquefiable deposit during earthquakes," Kyoto University, Japan.

Peck, R.B. [1990]. "fifty years of lateral earth support," *Design and Performance of Earth Retaining Structures, Geotechnical Special Publication No.25, ASCE*, pp.1-7.

Porcella, R.L. [1980] "*Atypical accelerograms recorded during recent earthquakes,*" Seismic Engineering Program Report, 1-7.

Rollins, K.M., Peterson, K.T. & Weaver, T.J. [1998]. "Lateral load behavior of full-scale pile group in clay," *Journal of Geotechnical and Geoenvironmental Engineering,* Vol.124, No.6, pp.468-478.

Sawada, S. [2003] "*A new look at Level 1 earthquake motions for performance-based design of civil engineering structures,"* Japan Society of Civil Engineers, http://www.jsce.or.jp/committee/eec2/taishin/index.html.

Schnabel, P.B., Lysmer, J. & Seed, H.B. [1972] "*SHAKE A Computer program for earthquake response analysis of horizontally layered sites,"* Berkeley, University of California, Berkeley, Report No. EERC72-12.

SEAOC [1995] "*Performance based seismic engineering of buildings,"* Sacrament, California, Structural Engineers Association of California

Seed, H.B. & Idriss, I.M. [1970] "*Soil moduli and damping factors for dynamic response analyses,"* Berkeley, University of California, Berkeley, Report No. EERC70-10.

Snyder, J.L. [2004]. "Full-scale lateral-load tests of a 3x5 pile group in soft clays and silts," Brigham young university, USA.

Steedman, R.S. [1998]. "Seismic design of retaining walls," *Geotechnical Engineering, Proc. Institution of Civil Engineers,* Vol.131, pp.12-22.

Sugito, M., Goda, H. & Masuda, T. [1994]. "Frequency dependent equi-linearized technique for seismic response analysis of multi-layered ground," *Journal of Geotechnical Engineering, JSCE,* Vol.493, No.III-27, pp.49-58 (in Japanese).

Terzaghi, K. [1943] "*Theoretical Soil Mechanics,"* New York, John Wiley and Sons, pp.510.

Tobita, T., Iai, S., Chairullah, B. & Asper, W. [2006]. "Reconnaissance report of the 2004 Sumatra-Andaman, Indonesia, Earthquake - Damage to geotechnical works in Band Aceh and Meulaboh," *Journal of Natural Disaster Science,* Vol.28, No.1, pp.35-41.

Tobita, T., S., I. & Iwata, T. [2010]. "Numerical analysis of trampoline effect in extreme ground motion," *Proc. 5th International Conference on Recent Advances in Geotechnical Earthquake Engineering and Soil Dynamics,* San Diego.

Tsuchida, H., Kurata, E. & Sudo, K. [1969] "*Strong-motion earthquake records on the 1968 Tokachi-oki earthquake and its aftershocks,"* Yokosuka, Japan, Port and Harbour Research Institute, 1-476.

Yoshida, N. & Iai, S. [1998]. "Nonlinear site response and its evaluation and prediction," IN Irikura, K., Kudo, K., Okada, K. & Sasatani, T. (Eds.) *The Second International Symposium on the Effects of Surface Geology on Seismic Motion,* Yokohama, Japan, A.A.Balkema, pp.71-90.

Zeghal, M. & Elgamal, A.W. [1994]. "Analysis of site liquefaction using earthquake records," *Journal of Geotechnical Engineering, ASCE,* Vol.120, No.6, pp.996-1017.

Zeghal, M., Elgamal, A.W., Tang, H.T. & Stepp, J.C. [1995]. "Lotung downhole array. II: evaluation of soil nonlinear properties," *Journal of Geotechnical Engineering, ASCE,* Vol.121, No.GT4, pp.363-378.